Ocean Radiant Heating. Part II: Parameterizing Solar Radiation Transmission through the Upper Ocean

J. CARTER OHLMANN

Scripps Institution of Oceanography, University of California, San Diego, La Jolla, California

DAVID A. SIEGEL

*Institute for Computational Earth System Science, Department of Geography, and
Donald Bren School of Environmental Science and Management, University of California, Santa Barbara,
Santa Barbara, California*

ABSTRACT

Accurate determination of sea surface temperature (SST) is critical to the success of coupled ocean–atmosphere models and the understanding of global climate. To accurately predict SST, both the quantity of solar radiation incident at the sea surface and its divergence, or transmission, within the water column must be known. Net irradiance profiles modeled with a radiative transfer model are used to develop an empirical solar transmission parameterization that depends on upper ocean chlorophyll concentration, cloud amount, and solar zenith angle. These factors explain nearly all of the variations in solar transmission. The parameterization is developed by expressing each of the modeled irradiance profiles as a sum of four exponential terms. The fit parameters are then written as linear combinations of chlorophyll concentration and cloud amount under cloudy skies, and chlorophyll concentration and solar zenith angle during clear-sky periods. Model validation gives a climatological rms error profile that is less than 4 W m^{-2} throughout the water column (when normalized to a surface irradiance of 200 W m^{-2}). Compared with existing solar transmission parameterizations this is a significant improvement in model skill. The two-equation solar transmission parameterization is incorporated into the TOGA COARE bulk flux model to quantify its effects on SST and subsequent rates of air–sea heat exchange during a low wind, high insolation period. The improved solar transmission parameterization gives a mean 12 W m^{-2} reduction in the quantity of solar radiation attenuated within the top few meters of the ocean compared with the transmission parameterization originally used. This results in instantaneous differences in SST and the net air–sea heat flux that often reach 0.2°C and 5 W m^{-2}, respectively.

1. Introduction

Ocean–atmosphere heat exchange in the tropical Pacific is a key process in regulating global climate. The Tropical Ocean and Global Atmosphere (TOGA) Coupled Ocean–Atmosphere Response Experiment (COARE) was designed in part to improve the understanding of air–sea fluxes in the western equatorial Pacific Warm Water Pool (WWP: Webster and Lukas 1992). Much effort in TOGA COARE has been spent with the computation of air–sea fluxes from bulk meteorological measurements for low wind environments (e.g., Fairall et al. 1996a,b; Weller and Anderson 1996). This requires thorough knowledge of the upper ocean heat budget as ocean thermal processes are tightly coupled with air–sea heat exchange (e.g., Smyth et al. 1996; Wijesekera and Gregg 1996; Fairall et al. 1996a; Cronin and McPhaden 1997).

Radiant heating is the largest term in the heat budget for the WWP and is unique in that it acts beyond boundaries. In situ irradiance data recorded during TOGA COARE indicate that between 60% and 90% of the solar energy reaching the sea surface is attenuated within the top 10 m of the ocean (Ohlmann et al. 1998). Such a discrepancy in solar transmission can result in a radiant heating rate difference of more than 0.12°C day^{-1} for the 10-m layer (based on a climatological surface irradiance of 200 W m^{-2}). Variations in the transmission of solar radiation can also influence the upper ocean heat budget indirectly, through water column stability (Ohlmann et al. 1996; Schneider et al. 1996; Ohlmann et al. 1998). The study by Schneider et al. (1996) states "mixing due to penetrative radiation is a central mixing mechanism for the western Pacific warm pool." Thus, both the quantity of incident solar irradiance and the

Corresponding author address: Dr. Carter Ohlmann, Scripps Institution of Oceanography, University of California, San Diego, 9500 Gilman Dr., Code 0230, La Jolla, CA 92093-0230.
E-mail: cohlmann@ucsd.edu

manner in which the irradiance is absorbed within the water column must be known to successfully model upper ocean thermal evolution (Denman 1973; Price et al. 1986; Fairall et al. 1996a; Ohlmann et al. 1996).

An optically based dataset collected during TOGA COARE has been used to estimate the range of variation in solar transmission and identify the factors which regulate transmission changes on mixed layer depth scales (Siegel et al. 1995; Ohlmann et al. 1998). The dataset has led to an improved mean solar transmission parameterization for the WWP aiding TOGA COARE investigators in heat budget work (e.g., Smyth et al. 1996; Wijesekera and Gregg 1996; Cronin and McPhaden 1997). The COARE in-water irradiance data is limited to the visible wavebands, those relevant to solar transmission beyond ~10 m (Siegel et al. 1995). Accurate measurements of irradiance within the top 5 m of the ocean are hampered by rapid variations in sea-surface height and difficulty in constructing full spectral detectors. Radiant heating studies for the near-surface layer of the ocean must therefore rely on model results that can resolve both depth variations on the smallest scales and the wavelengths that e-fold on these scales.

In-water radiative transfer calculations were recently used to generate full spectral radiance profiles over a variety of atmospheric and oceanic conditions (Ohlmann et al. 2000; hereafter referred to as OSM). These simulated profiles show that variations in solar transmission within the top few meters of the ocean can exceed 40 W m^{-2} (based on a surface irradiance of 200 W m^{-2}) due primarily to changes in chlorophyll concentration, cloud amount, and solar zenith angle. Here, the simulated profiles present in OSM are used to develop an improved solar transmission parameterization that is physically and biologically based and can be used for the complete set of conditions found in open ocean waters. The derived parameterization is then incorporated into the TOGA COARE bulk flux formula (Fairall et al. 1996b) to assess the sensitivity of upper ocean evolution and air–sea heat fluxes to the near-surface solar transmission parameterization.

2. Background

a. Solar transmission parameterizations

The rate at which solar radiation heats an upper ocean layer of depth z, or radiant heating rate (RHR), is

$$\text{RHR}(z) = \frac{E_n(0^-) - E_n(z)}{\rho c_p z}, \qquad (1)$$

where $E_n(0^-)$ is the total (spectrally integrated) net flux of solar radiation just beneath the sea surface ($z = 0$), $E_n(z)$ is the total net solar flux at the base of the layer (depth z), ρ is the density of seawater, and c_p is the specific heat of seawater. The change in solar flux over depth can be expressed with a solar transmission parameter, Tr, as

$$E_n(0^-) - E_n(z) = E_d(0^+)[\text{Tr}(0^-) - \text{Tr}(z)], \qquad (2)$$

where $E_d(0^+)$ is the total solar irradiance incident on the sea surface, and solar transmission is defined as

$$\text{Tr}(z) = \frac{E_n(z)}{E_d(0^+)} \cong \sum_{i=1}^{n} A_i \exp(-K_i z). \qquad (3)$$

Solar transmission gives the fraction of the incident surface irradiance that exists at depth and can be parameterized as a sum of exponentials. This definition of transmission includes the effects of the sea surface albedo (α). An in-depth development of solar transmission is presented in OSM. Similar equations are given in Paulson and Simpson (1977, 1981), Woods et al. (1984), Morel and Antoine (1994), and used by the Price et al. (1986), Fairall et al. (1996b), and other upper ocean models. The crux of the ocean radiant heating problem lies in determining coefficients A_i and exponents K_i for solar transmission parameterizations, and resolving variations in these parameters.

Solar transmission parameterizations can be divided into two general classes, visible and full spectral models. Visible models are developed from irradiance values confined mainly to the visible portion of the solar spectrum (~400–700 nm; e.g., Kraus 1972; Paulson and Simpson 1977; Woods et al. 1984; Siegel and Dickey 1987, Morel 1988; Ohlmann et al. 1996, 1998). They are appropriate for applications in bio-optics, or for determining solar fluxes beyond the top few meters where only visible energy remains. Transmission parameterizations for visible energy may have as few as one, or nearly 100 exponential terms. Coefficient and exponent values are generally determined empirically as a function of the Jerlov water type or upper ocean chlorophyll biomass which strongly influences attenuation of visible energy (Jerlov 1976; Smith and Baker 1978; Morel 1988). Full spectral solar transmission models resolve the entire solar spectrum (250–2500 nm) making them suitable for radiant heating applications within the top few meters of the ocean where near-infrared energy can be a significant fraction of the total irradiance (e.g., Paulson and Simpson 1981; Morel and Antoine 1994). Parameters for full spectral models can be completely empirical or based on radiative transfer theory. Generally, full spectral transmission models are completely invariant. The only full spectral parameterization that allows variations does so by writing model parameters in terms of chlorophyll concentration in the visible wavebands and in terms of solar zenith angle in the near-infrared wavebands (Morel and Antoine 1994). Although an improvement over invariant models, Morel and Antoine represent the entire near-infrared spectral region as a single exponential term making their parameterization erroneous at the shallowest depths. A full spectral solar transmission model that accurately resolves the upper few meters has yet to be developed.

b. Simulated irradiance profiles

A set of full spectral irradiance profiles generated with the HYDROLIGHT radiative transfer model allows for quantification of chlorophyll concentration, cloud amount, solar zenith angle, and wind speed effects on variations in the transmission of solar radiation through the upper ocean (OSM). The HYDROLIGHT model solves the one-dimensional monochromatic radiative transfer equation for a given radiance distribution incident at the sea surface, upper ocean optical properties, and sea surface and bottom boundary conditions (Mobley 1989, 1994). A complete description of the enhanced full spectral HYDROLIGHT model used to simulate irradiance profiles for this study is given in OSM.

HYDROLIGHT simulations have been performed for chlorophyll concentrations (chl) of 0.03, 0.1, 0.3, 1.0, and 3.0 mg m^{-3}; solar zenith angles (θ) of 0°, 15°, 30°, 45°, 60°, and 75°; cloud indices (CI) of 0, 0.2, 0.4, 0.6, and 0.9; and a 2 m s^{-1} wind speed ($n = 150$). Cloud index is a radiometric quantification of clouds, defined as one minus the ratio of the incident irradiance to clear sky irradiance (Gautier et al. 1980; Siegel et al. 1999). Variations in wind speed have relatively little influence on model results (OSM). This set of independent parameters spans the range of conditions that characterizes open ocean waters. The complete set of simulated transmission profiles is shown and discussed in OSM. A subset of the modeled profiles, along with solar transmission profiles from the Paulson and Simpson (1981), the Soloviev (1982), and the Morel and Antoine (1994) parameterizations are shown in Fig. 1. The simulated transmission profiles give the range of values that can be expected for an upper ocean layer with 0.3 mg m^{-3} of chlorophyll (a typical open ocean value). Solar transmission values vary by 0.24 and 0.09 at depths of 10 cm and 5 m, respectively (Fig. 1). These ranges in transmission correspond to absolute solar flux differences 48 and 18 W m^{-2} (based on a climatological surface irradiance of 200 W m^{-2}) and are due primarily to changes in cloud amount, and solar zenith angle (OSM). The range of solar transmission values can be even larger if chlorophyll concentration changes are considered. It is these variations in transmission which we attempt to capture in the parameterization developed here.

3. Analysis of simulated irradiance profiles

Solar transmission parameterizations represented as a single curve fit to a complete set of irradiance profiles may be adequate for generating a mean profile, but fail to resolve spatial and temporal variations (e.g., Paulson and Simpson 1977, 1981; Ohlmann et al. 1998; OSM). For the parameterization developed here, curves with four exponential terms [Eq. (3); $n = 4$] are fit to each of the simulated transmission profiles using a gradient-expansion type algorithm (Bevington and Robinson 1992). Four term fits give r^2 values which exceed 0.999,
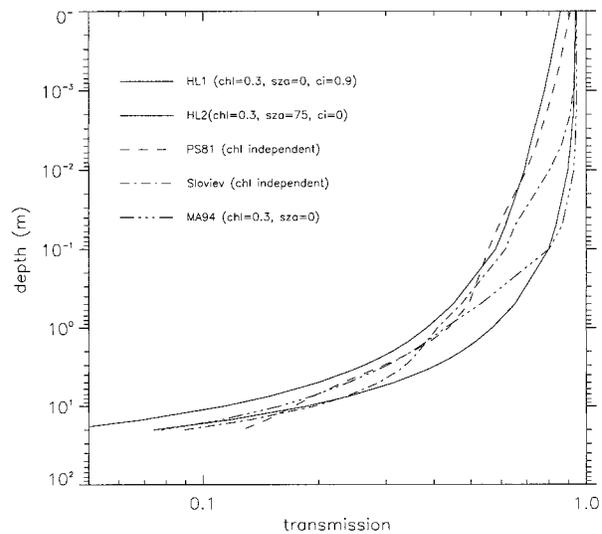

FIG. 1. Solar transmission [Eq. (3)] determined from modeled irradiance profiles for the clear sky, 75° solar zenith angle case (low transmission) and for the 0.9 cloud index, 0° solar zenith angle case (high transmission). These curves span the complete range of transmission values present in the model results for an upper ocean chlorophyll concentration of 0.3 mg m^{-3}. Also shown are solar transmission profiles from the Paulson and Simpson (1981), Soloviev (1982), and Morel and Antoine (1994) parameterizations.

and rms error estimates of order 0.001 within the top 20 m of the ocean. By comparison, rms error estimates for three term exponential fits are an order of magnitude larger, and the addition of a fifth term results in only slight error improvements. Histograms giving the distribution for each of the eight "fit parameters" are shown in Fig. 2. The largest variation exists in the K_1, K_2, and K_3 parameters, followed by K_4 and A_4. The remaining parameters (A_1, A_2, and A_3) are much more concentrated around their respective means.

Fit parameters can be interpreted as representing the fraction of the total irradiance incident at the sea surface (A_i) and its corresponding *e*-folding depth (K_i^{-1} m). Although the parameters are not strictly representative of specific spectral regions, hypotheses regarding the physical and biological factors responsible for their variations can still be developed. Relationships between fit parameters and the independent variables chl, CI, and $1/\cos(\theta)$ are quantified in Table 1, and illustrated in Figs. 3–5, respectively. Correlation coefficients have been calculated using fit parameters from the entire set of simulated profiles, from only clear sky profiles, and from only cloudy sky profiles. This was done to address the role of solar zenith angle ($1/\cos\theta$) which has a significant influence on solar transmission during clear sky periods (OSM).

The most statistically significant relationships involving chlorophyll concentration are with the K_i parameters for which *e*-folding depths are greater than ~ 1 m (K_1, K_2; Table 1, Fig. 3). Strong correlations between K_1, K_2, and chlorophyll are expected because chloro-
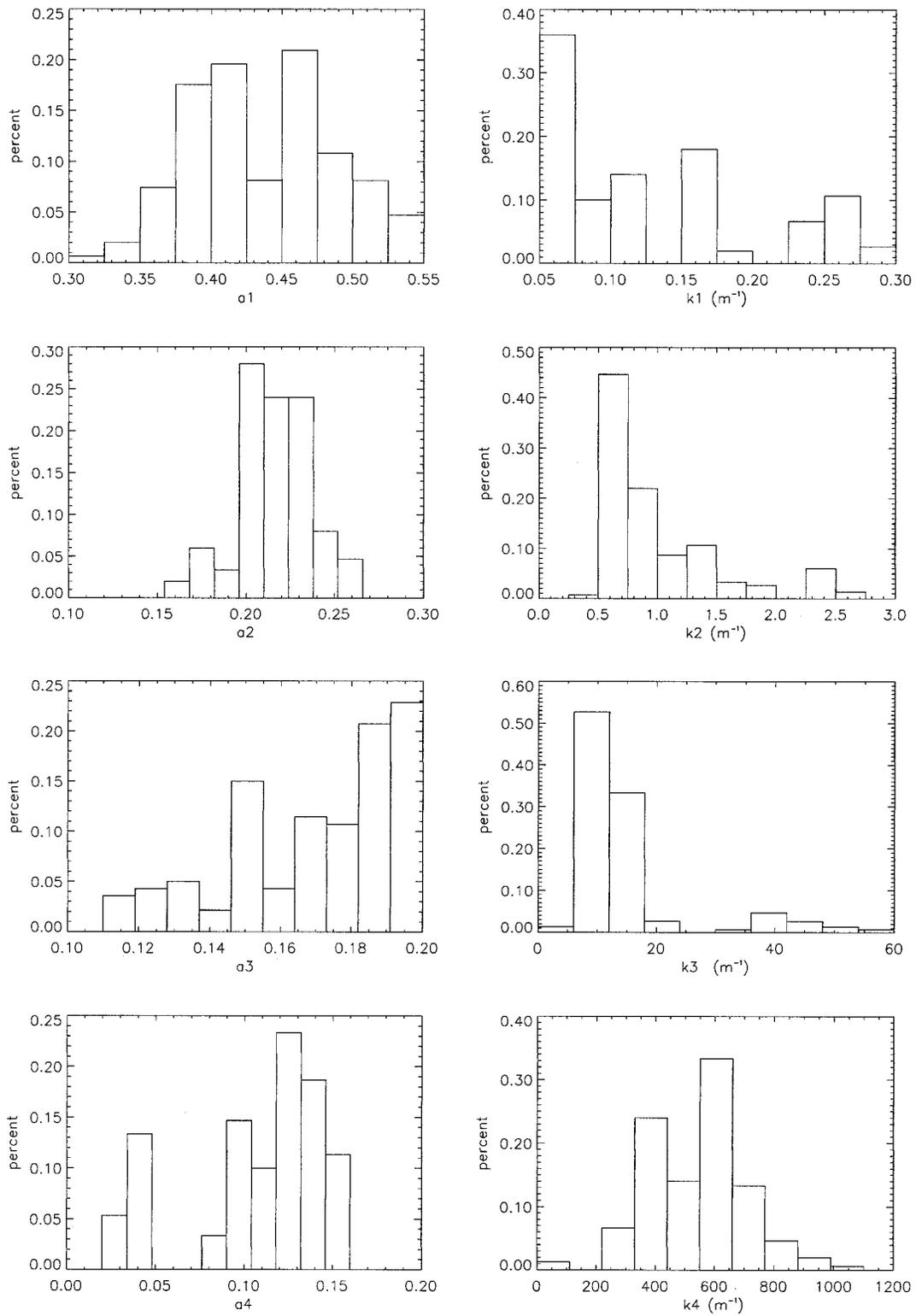
FIG. 2. Distributions of the 8 parameters (A_{1-4}, K_{1-4}) determined by curve fits to the individual solar transmission profiles [$n = 150$; Eq. (3)].

TABLE 1. Linear correlation coefficients (r) between fit parameters and independent variables. Values have been determined using all simulated solar transmission profiles ($n = 150$), just the profiles simulated during cloudy skies (CI > 0.1; $n = 120$) and just the profiles simulated during clear skies ($n = 30$).

	Chlorophyll concentration			Cloud index		$1/\cos\theta$		
	All	Cloud	Clear	All	Cloud	All	Cloud	Clear
A_1	0.57	0.57	0.75	0.58	0.58	−0.16	−0.08	−0.51
A_2	−0.50	−0.49	−0.60	0.37	0.43	−0.24	−0.21	−0.37
A_3	−0.72	−0.72	−0.72	−0.06	−0.07	−0.03	−0.01	−0.10
A_4	0.15	0.16	0.15	−0.93	−0.94	0.06	0.10	−0.35
K_1	0.97	0.97	0.97	−0.05	−0.05	0.03	0.01	0.08
K_2	0.67	0.67	0.74	−0.31	−0.31	−0.02	−0.01	−0.05
K_3	0.52	0.54	0.62	−0.41	−0.41	−0.09	−0.06	−0.18
K_4	0.16	0.13	0.58	−0.90	−0.89	0.03	0.02	0.13

phyll is a primary regulator of light attenuation for the visible wavebands which exhibit such decay scales (e.g., Smith and Baker 1978; Morel 1988; Kirk 1994; OSM). The correlations between chlorophyll and K_i parameters decrease as the value of K_i increases because chlorophyll has little influence on attenuation of the red and near-infrared wavebands (OSM). Although no biophysical relationships between chlorophyll concentration and shape of the incident irradiance spectrum are included in the radiative transfer calculations, results show statistically significant correlations between chlorophyll and the A_1, A_2, and A_3 parameters (Table 1, Fig. 3). This is a result of spectral narrowing which occurs with depth. The A_1 parameter increases with chlorophyll concentration so that energy in the wavelengths with the largest e-folding depths can still make it to depth. The positive correlation between A_1 and chl can be viewed as a partial offset to the K_1 increase with chl, which occurs because chl effects are spectrally dependent. The negative correlations between A_2 and chl, and A_3 and chl are due to compensation for the A_1 increase. They occur because the A_i represent fractions of the total incident irradiance and must sum to $1 - \alpha$, where α is the sea surface albedo (OSM). Correlation coefficients between fit parameters and chlorophyll concentration show little change when clear sky and cloudy sky profiles are considered separately (Table 1).

Linear correlation coefficients between cloud index and the fit parameters are given in Table 1 and illustrated in Fig. 4. Significant relationships between cloud amount and the A_i parameters are expected because clouds alter the fraction of the total energy which exists in the various wavebands (Siegel et al. 1999; OSM). As cloud index increases, less of the incident energy is in wavebands with e-folding scales of order mm (A_4; the near-infrared spectral region), and more of the energy is contained in wavebands with e-folding scales of order 10 cm and greater (A_1, A_2; roughly the visible spectral region). Thus, statistically significant positive correlations exist between cloud index and the A_1 and A_2 parameters, and a significant negative correlation exists with A_4 (Table 1, Fig. 4). Cloud index is inversely correlated with the K_i parameters, and correlation magnitudes decrease with e-folding depth. These correlations

are due to an overall increase in transmission, which exists with clouds due to the enhancement of energy in the deep penetrating visible wavebands relative to the total irradiance (OSM). Correlation coefficients between fit parameters and cloud index change only slightly when clear sky profiles are excluded from the regression.

Relationships between $\cos^{-1}\theta$, a path length amplification factor, and the eight fit parameters are illustrated in Fig. 5, and corresponding correlation coefficients are given in Table 1. Statistically significant correlations exist between $\cos^{-1}\theta$ and the A_1, A_2, and A_4 parameters when only the clear sky profiles are considered. Under a cloudy sky, the incident irradiance distribution is largely diffuse and therefore has little dependence on solar zenith angle. The role of solar zenith angle on transmission is manifest primarily through sea-surface albedo (OSM). A decrease in the sum of the A_i parameters indicates a reduction in the total amount of energy that exists just beneath the sea surface, and this is exactly the role of sea surface albedo. Negative correlations between $\cos^{-1}\theta$ and the A_i parameters support this connection. The strongest correlation involving $\cos^{-1}\theta$ is with the A_1 parameter, and it is the spectral region represented by A_1 (those wavebands which e-fold on a K_1^{-1} depth scale) that exhibits the greatest change in surface albedo with solar zenith angle (OSM). There are no statistically significant correlations between $\cos^{-1}\theta$ and the K_i parameters (Table 1). The correlations discussed here suggest that $\cos^{-1}\theta$ is an important variable in explaining transmission variations during clear sky periods, and cloud index is important under cloudy skies. Chlorophyll concentration must be considered for both clear and cloudy sky conditions.

4. The solar transmission model

Based upon the correlation results, multivariate least squares analysis is used to model the fit parameters in terms of the independent predictor variables chlorophyll concentration, cloud index, and solar zenith angle with an equation of the form

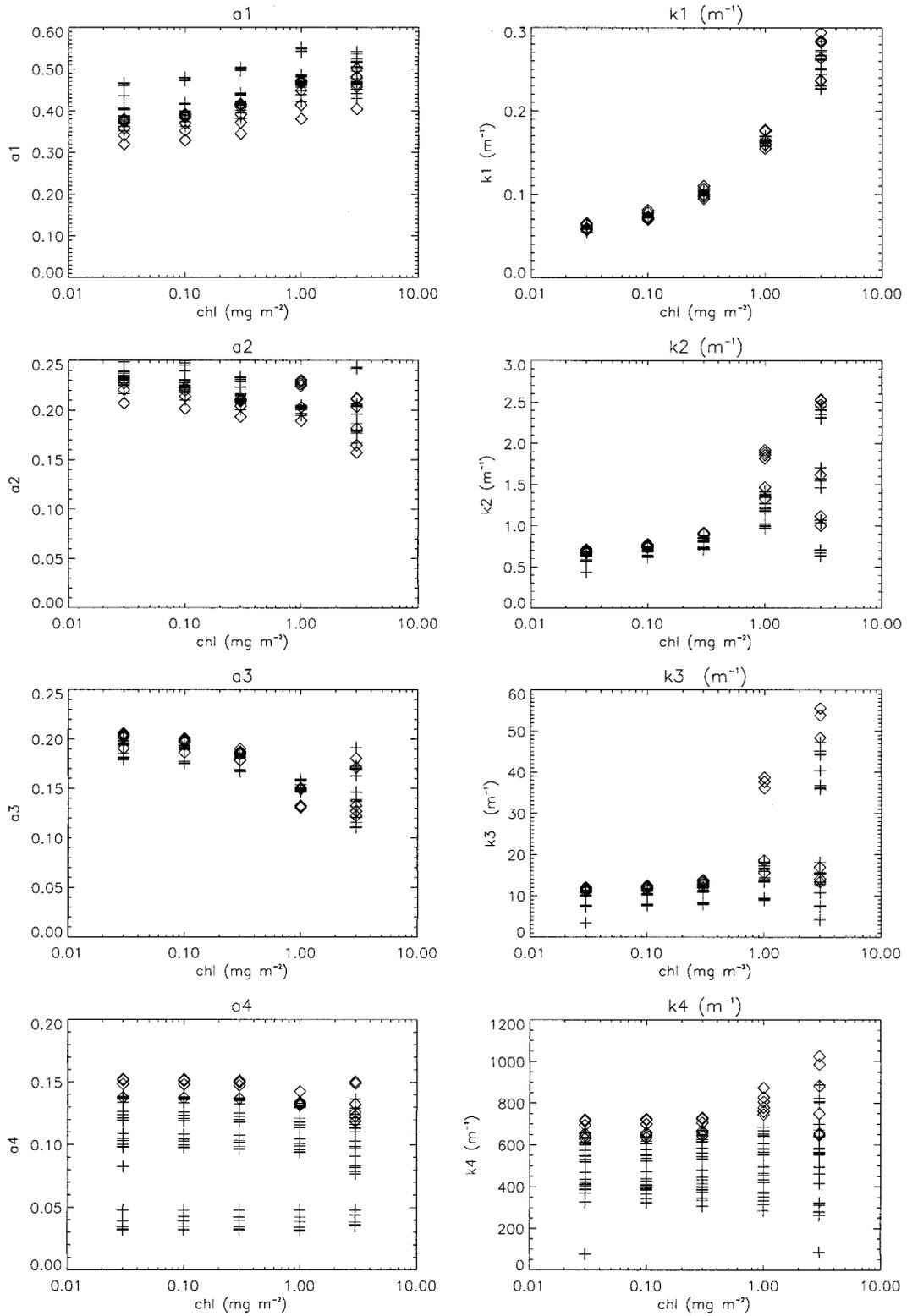$$y = C_1\text{chl} + C_2\text{CI} + C_3\cos^{-1}\theta + C_4, \qquad (4)$$

FIG. 3. Relationships between the eight parameters determined by curve fits to the individual solar transmission profiles [Eq. (3)] and the independent variable chlorophyll concentration. Correlation coefficients from linear regressions are given in Table 1. Diamonds indicate values from fits to clear sky profiles.
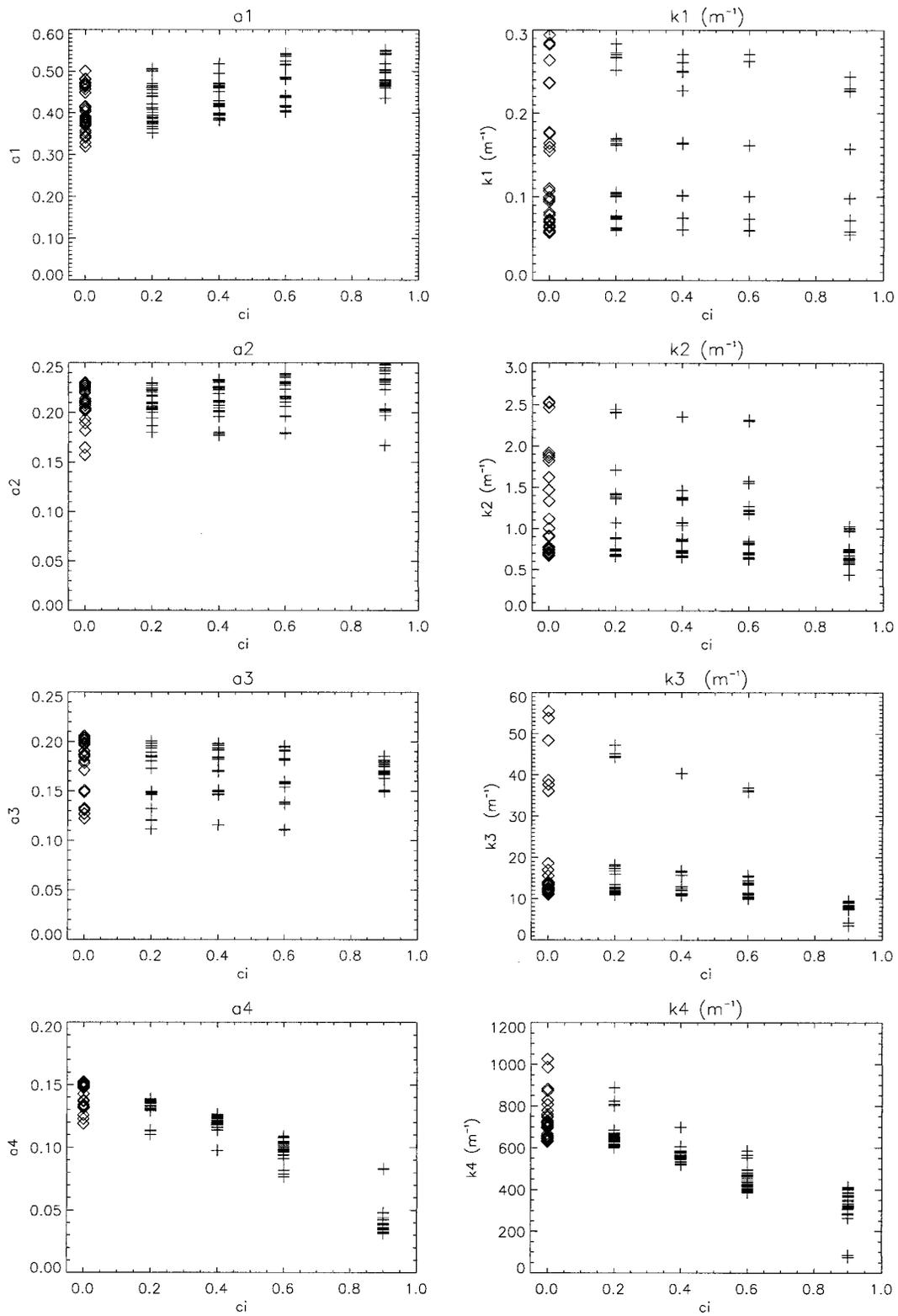
Fig. 4. As in Fig. 3 but for relationships between fit parameters and the independent variable cloud index.
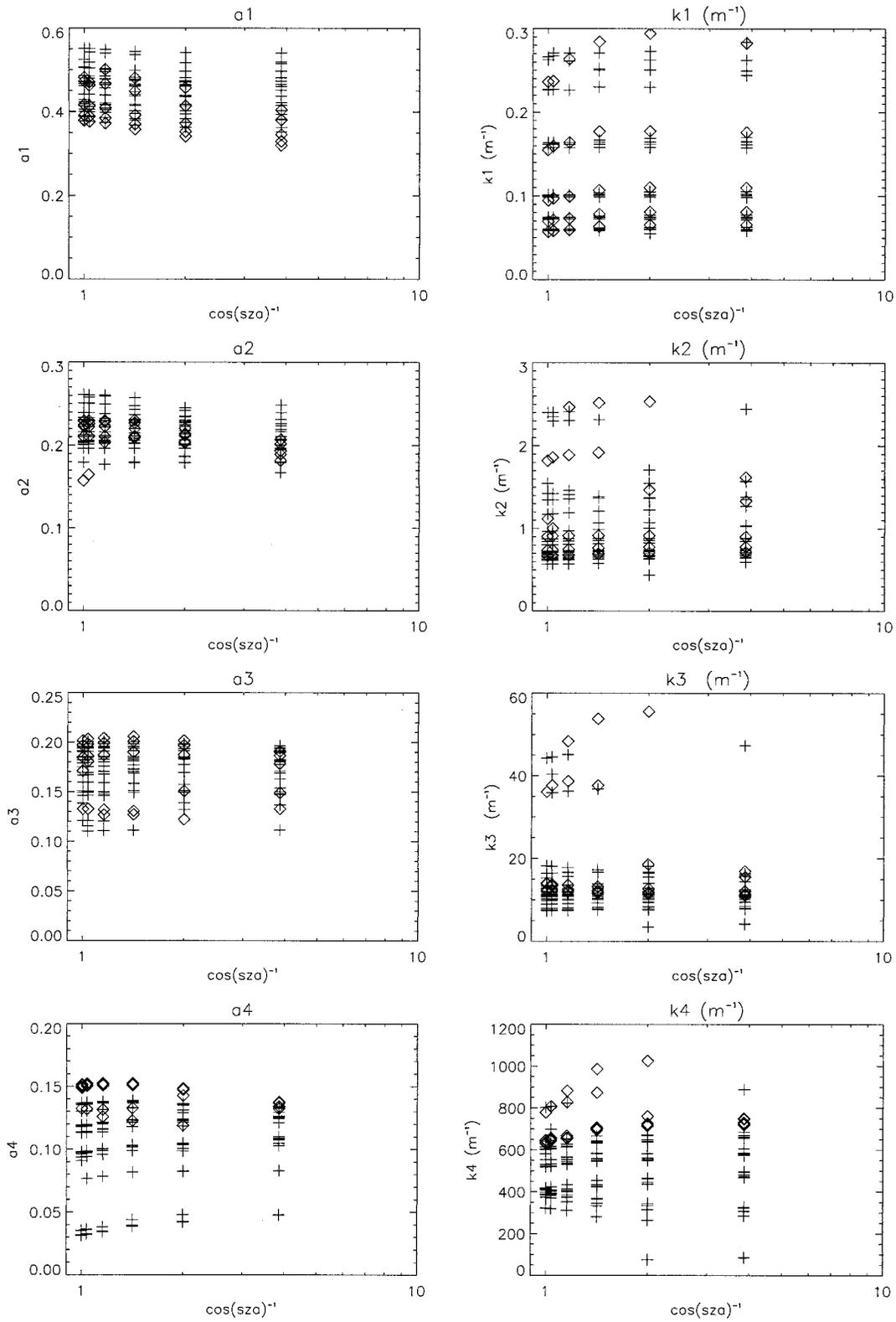
FIG. 5. As in Fig. 3 but for relationships between fit parameters and the independent variable solar zenith angle (represented as $\cos^{-1}\theta$).
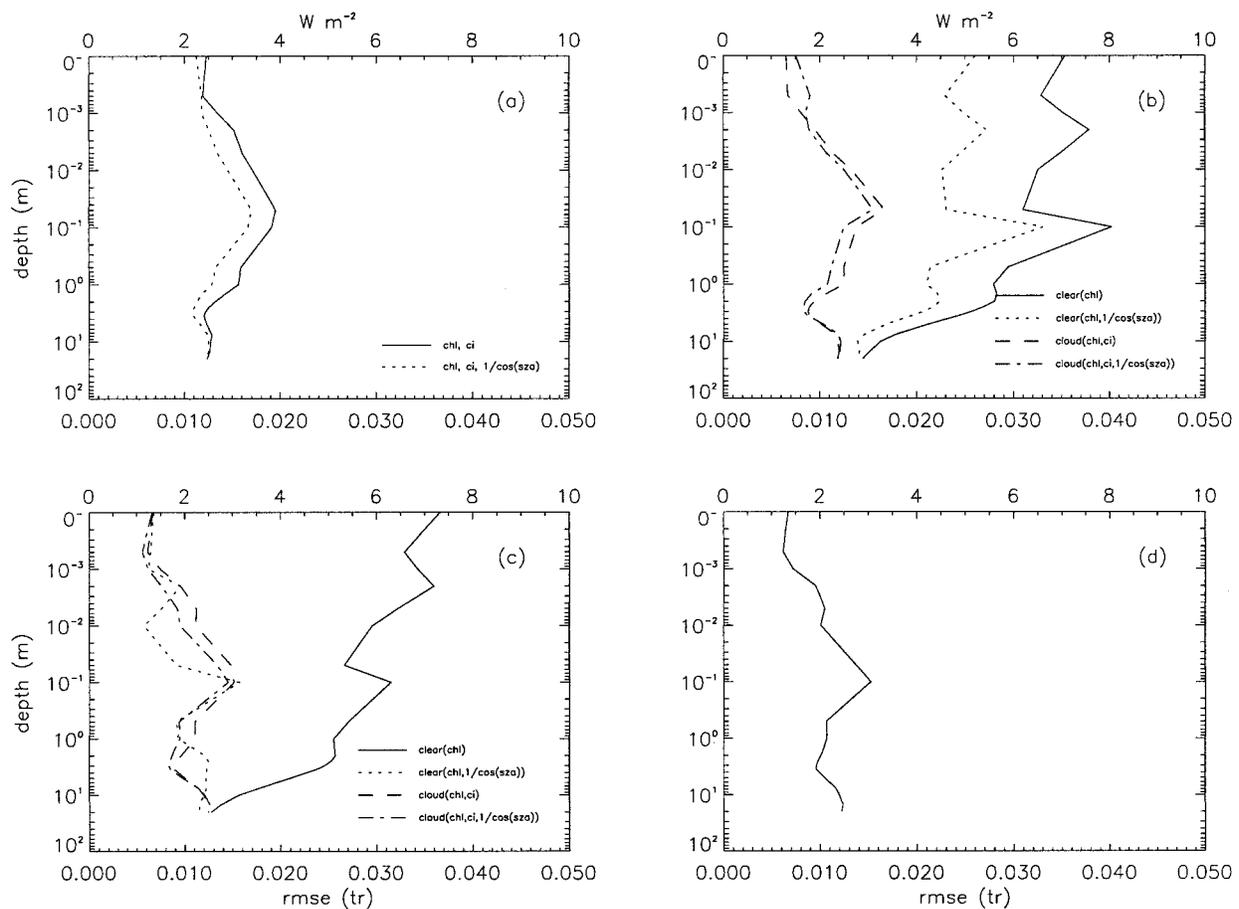
FIG. 6. Ensemble-averaged rms error profiles for variations of the general solar transmission model defined here [Eq. (4)]: (a) the empirical model is determined with the entire set of simulated profiles and cross validated against the entire set of simulated profiles; (b) the empirical model is determined using the entire set of simulated profiles and cross-validated against the clear sky profiles (solid and dotted curves), and cloudy sky profiles (dashed and dot–dash curves) separately; (c) the set of clear sky profiles is used to determine and cross-validate an empirical clear sky model, and the set of cloudy sky profiles is used to determine and cross-validate a cloudy sky model; (d) the resultant rms error profile from the two-equation model (see text). Independent parameters included in each of the tested models are indicated as chl, for chlorophyll concentration; CI, for cloud index; and $1/\cos(\theta)$, for $\cos^{-1}\theta$.

where y represents the fit parameters (A_i and K_i). Once the fit parameters are determined, Eq. (3) can be solved for solar transmission as a function of depth, and net solar irradiance profiles can be determined given the surface incident irradiance. The empirical solar transmission model developed here is tested against the simulated irradiance profiles using a "leave-one-out" cross-validation procedure (Efron and Tibshirani 1993). Cross-validation, a standard method for computing statistical model skill, is carried out by individually excluding each of the simulated profiles and refitting the model with the remainder of the profiles. The model is then used to predict the excluded profile. This procedure gives a set of 150 individual error profiles that can be combined for a single ensemble average rms error profile.

An empirical transmission model based on the complete set of simulated irradiance profiles, and dependent upon chl, CI, and θ [Eq. (4)], gives an rms error profile less than 0.018 at all depths (Fig. 6a, dotted line). When a model is developed without a solar zenith angle dependency [Eq. (1) without the $C_3 \cos^{-1}\theta$ term], rms error increases by $\sim$0.02 for most depths (Fig. 6a, solid line). This slight decrease in skill without the $\cos^{-1}\theta$ dependency is due to the large number of cloudy sky profiles used in the cross-validation scheme and that only weak relationships exist between $\cos^{-1}\theta$ and the fit parameters for cloudy sky periods (Table 1). Results given in OSM and the statistical analysis performed here both indicate that solar zenith angle is important in regulating solar transmission only during clear sky periods. It is thus necessary to quantify the skill of the empirical model without the $\cos^{-1}\theta$ dependency in prediction of solar transmission under clear skies. This is done by cross-validating against only clear sky profiles. Figure 6b shows rms error profiles for cross-validation of the empirical model with and without the $\cos^{-1}\theta$ dependency against the clear sky and cloudy sky profiles separately.

TABLE 2. Linear regression coefficients for determination of the eight model parameters used in the two-equation solar transmission parameterization presented here, which has the general form $y = C_1 \text{chlorophyll} + C_2 \text{CI} + C_3 \cos\theta + C_4$: (a) gives coefficients for the cloudy sky model, which depends on chlorophyll concentration and cloud amount [Eq. (5a)]. (b) gives coefficients for the clear sky model, which depends on chlorophyll concentration and solar zenith angle [$\cos(\theta)^{-1}$; Eq. (5b)]. Also shown is the explained variance for each dependent parameter.

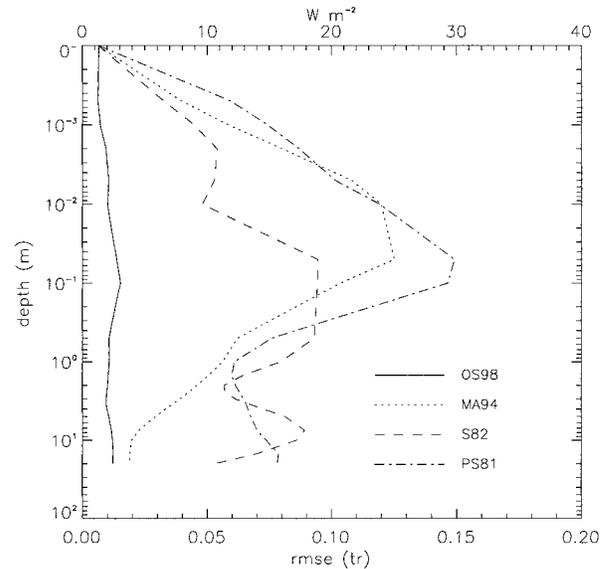|	C_1	C_2	C_3	C_4	r^2
		(a)			
A_1	0.026	0.112	—	0.366	0.66
A_2	−0.009	0.034	—	0.207	0.42
A_3	−0.015	−0.006	—	0.188	0.52
A_4	−0.003	−0.131	—	0.169	0.89
K_1	0.063	−0.015	—	0.082	0.95
K_2	0.278	−0.562	—	1.02	0.54
K_3	3.91	−12.91	—	16.62	0.46
K_4	16.64	−478.28	—	736.56	0.82
		(b)			
A_1	0.033	—	−0.025	0.419	0.82
A_2	−0.010	—	−0.007	0.231	0.49
A_3	−0.019	—	−0.003	0.195	0.52
A_4	−0.006	—	−0.004	0.154	0.49
K_1	0.066	—	0.006	0.066	0.94
K_2	0.396	—	−0.027	0.886	0.56
K_3	7.68	—	−2.49	17.81	0.42
K_4	51.27	—	13.14	665.19	0.35

FIG. 7. Ensemble-averaged rms error profiles for the two-equation model presented here (solid line), the Morel and Antoine (1994: dotted line), the Soloviev (1982: dashed line), and the Paulson and Simpson (1981: dash–dot line) solar transmission parameterizations.

Note that when only clear sky profiles are considered the $C_2\text{CI}$ term in Eq. (4) vanishes. Model skill is reduced (rms error exceeds 0.04 near 10 cm) when solar transmission profiles are modeled under clear skies without regard to θ (Fig. 6b, solid line). Even when an empirical model that includes a $\cos^{-1}\theta$ dependency [Eq. (4)] is determined using all profiles and validated against only clear sky profiles, rms error shows a significant increase (Fig. 6b, dotted line). By comparison, rms error profiles are mostly less than 0.015 when model validation is performed on only the cloudy sky profiles (Fig. 6b, dash and dot–dash lines).

To improve solar transmission model skill under clear skies two distinct empirical parameterizations are developed: one for cloudy skies and one for clear skies. This "two-equation model" uses the equation

$$y = C_1 \text{chl} + C_2 \text{CI} + C_4 \qquad (5a)$$

to represent the fit parameters (A_i and K_i) in terms of chl and cloud index for cloudy conditions and the equation

$$y = C_1 \text{chl} + C_3 \cos^{-1}\theta + C_4 \qquad (5b)$$

to represent the fit parameters in terms of chlorophyll and $\cos^{-1}\theta$ during clear sky periods. By defining two empirical parameterizations, model skill is substantially improved when computing solar transmission profiles during clear sky periods. Figure 6c shows that clear sky model error is substantially reduced when a separate clear sky parameterization is developed. Model rms error computed for the two-equation parameterization

never exceeds 0.015 and is mostly near 0.01, corresponding to absolute solar flux errors less than 3 W m^{-2} (based on a climatological surface irradiance of 200 W m^{-2}; Fig. 6d). The rms error estimates given here include effects of the sea surface albedo. Coefficients for the two-equation parameterization and a quantification of the explained variance in the fit parameters are given in Table 2.

5. Improvement over existing solar transmission parameterizations

The rms error profile computed for the two-equation parameterization (and illustrated in Fig. 6d) is shown in Fig. 7 along with rms error profiles determined by modeling the entire set of simulated profiles with the parameterizations of Paulson and Simpson (1981, hereafter PS81), Soloviev (1982, hereafter S82) and Morel and Antoine (1994, hereafter MA). The PS81 model is a sum of nine exponential terms with coefficients and exponents determined from laboratory experiments conducted in the early 1900s. The S82 model is based on measurements for Jerlov Type 1A water and has three exponential terms. The MA94 model has three exponential terms with exponents related to "zenith angle of the refracted sun rays" (near-infrared term) and chlorophyll concentration (visible terms). Profiles used for development of the MA model are from a hybrid parameterization based primarily on the bio-optical model of Morel (1988). The existing set of solar transmission parameterizations does not resolve transmission through the air–sea interface. Surface albedo values are computed separately as a function of solar zenith angle and

atmospheric transmittance using the Payne (1972) model. Ensemble average rms errors for the PS81, S82, and MA parameterizations are as large as 0.15, 0.09, and 0.13, respectively, corresponding to absolute solar flux values of between 18 and 30 W m^{-2} (Fig. 7). By comparison, the two-equation model developed here has an associated rms error profile everywhere <0.015, or nearly an order of magnitude smaller. Just beneath the sea surface the PS81, S82, and MA parameterizations all perform similarly as they rely on the same albedo values (Payne 1972). Surface albedo from the model presented here agrees well with Payne's values (OSM). The increase in model skill with depth beneath $\sim$1 m in the MA94 parameterization illustrates the importance of defining transmission in terms of chlorophyll concentration (Morel and Antoine 1994; OSM).

6. Influences on SST prediction and air–sea heat exchange

The effects of a much improved near-surface solar transmission model on upper ocean evolution and air–sea heat exchange are now investigated for a high insolation, low wind speed period using the TOGA COARE bulk flux algorithm (v2.5b: Fairall et al. 1996b). The algorithm, based upon the Liu et al. (1979) bulk flux parameterization, uses similarity theory to obtain turbulent air–sea heat fluxes from bulk meteorological variables. Key to the TOGA COARE bulk flux algorithm are "cool skin" and "warm layer" physics that relate ocean temperature at the air–sea interface (subsequently referred to as sea surface temperature or SST) to the bulk surface temperature measured somewhere near the surface (subsequently referred to as bulk temperature) via cool-skin and warm-layer temperature corrections (Fairall et al. 1996a). The cool-skin and warm-layer calculations are based on the Saunders (1967) and Price et al. (1986) models respectively, and discussed in detail by Fairall et al. (1996a).

The TOGA COARE bulk flux algorithm parameterizes solar transmission as a sum of exponential terms. Solar transmission model parameters for the warm-layer and cool-skin calculations are from the Soloviev (1982) and Paulson and Simpson (1981) parameterizations, respectively. Model parameters are based upon Jerlov water type, an obsolete index of upper ocean turbidity, and data that is more than 20-years old (Jerlov 1976). The bulk flux algorithm computes solar transmission through the air–sea interface separately by fixing sea surface albedo at 0.055, a value known to give instantaneous errors of up to $\pm$40 W m^{-2} (Coppin and Bradley 1995).

The effects of a physically and biologically based solar transmission parameterization on upper ocean thermal evolution and subsequent rates of air–sea heat exchange are investigated by replacing the transmission parameterization that exists in the original bulk flux model with the parameterization presented here. Specifically, the two-equation solar transmission model [Eq.

(5), Table 2] is used to determine the transmission parameters [Eq. (3)] at each time step as a function of upper ocean chlorophyll concentration and solar zenith angle (for clear sky periods) or chlorophyll concentration and cloud amount (for cloudy sky periods). Sea surface albedo is implicit to the improved transmission parameterization.

The TOGA COARE bulk flux model represents the absorption of solar radiation within the cool-skin and warm-layer as a fraction of the surface incident flux (Fairall et al. 1996a). Rather than computing the solar flux divergence, an average solar flux for a layer of depth δ is calculated as

$$\frac{1}{\delta} \int_0^{-\delta} (E_n(0^-) - E_n(z)) \, dz, \qquad (6)$$

following Saunders (1967). The solar transmission parameterization presented here is incorporated into the bulk flux model by substituting Eqs. (2) and (3) into Eq. (6) and carrying out the integration to give

$$f_w = \left[\sum_{i=1}^4 A_i z - \sum_{i=1}^4 A_i K_i^{-1} (1 - \exp(-K_i z)) \right] \bigg/ z. \qquad (7)$$

The result of the integration (f_w) is the average solar flux converted to thermal energy within the layer, defined as a fraction of the incident surface irradiance. This equation differs from that of Fairall et al. (1996a) by including the sea surface albedo. The definition of average solar flux presented in Eq. (7) enables the net heat flux (Q_{net}) for an upper ocean layer to be written as

$$Q_{net} = f_w E_d(0^+) + Q_{lw} + Q_{lat} + Q_{sen}, \qquad (8)$$

where terms on the right represent shortwave, longwave, latent, and sensible heat components, respectively.

Variations in near-surface solar transmission are of greatest importance during quiescent conditions when shear-driven mixing is at a minimum (e.g., Fairall et al. 1996a). Sensitivity to solar transmission is investigated for the January low wind period (5–15 January 1993) encountered during the TOGA COARE intensive observing period (IOP; Weller and Anderson 1996). The meteorological and oceanographic measurements used to force the TOGA COARE bulk flux algorithm during this time are from the improved meteorological instrument (IMET) mooring located in the western equatorial Pacific as part of TOGA COARE (Weller and Anderson 1996). These time-series (Fig. 8) are a subset of the data presented by Weller and Anderson. Mean values of wind speed and solar insolation for the 10 day period are 2.0 m s^{-1} and 204 W m^{-2}. The mean solar value is the same as that reported by Weller and Anderson (1996) for the entire IOP. Bulk temperature, measured at 0.45 m, has a mean value of 29.3°C and increases nearly 2°C during the study period.

Values of upper ocean chlorophyll concentration and cloud index used to drive the two-equation solar transmission model developed here are shown in Fig. 9. Up-
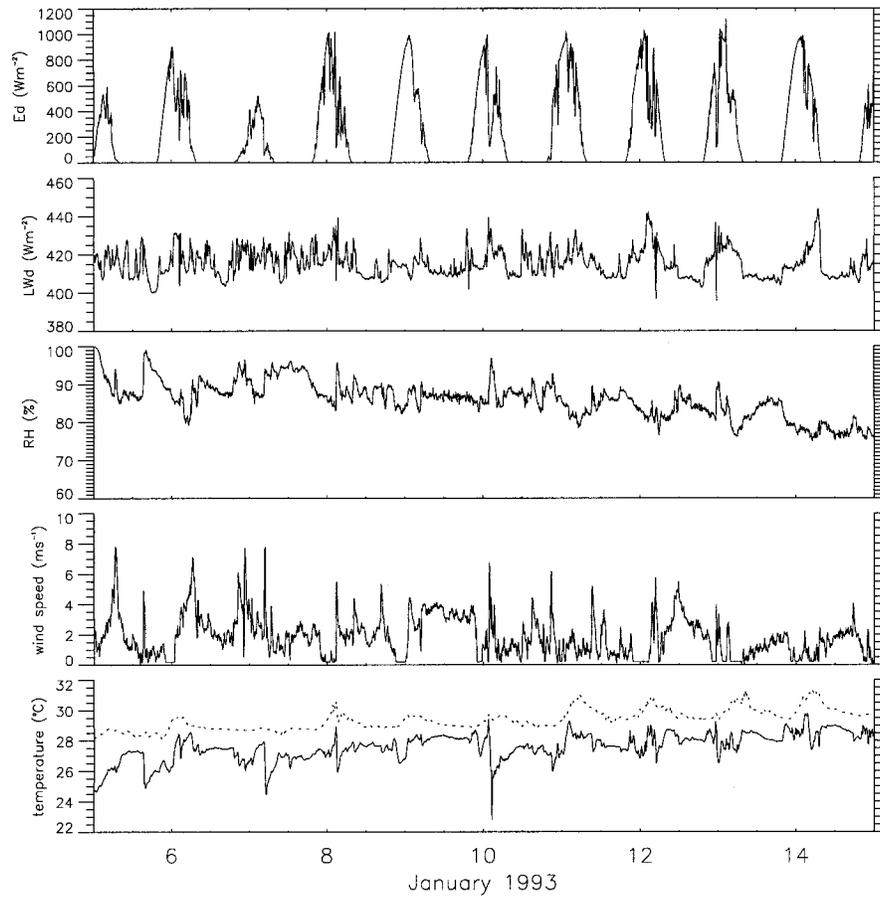
FIG. 8. Meteorological measurements made at the IMET mooring during TOGA COARE. The parameters are downwelling shortwave and longwave radiation at the sea surface, relative humidity, wind speed, air (solid line), and ocean (dotted line) temperature.
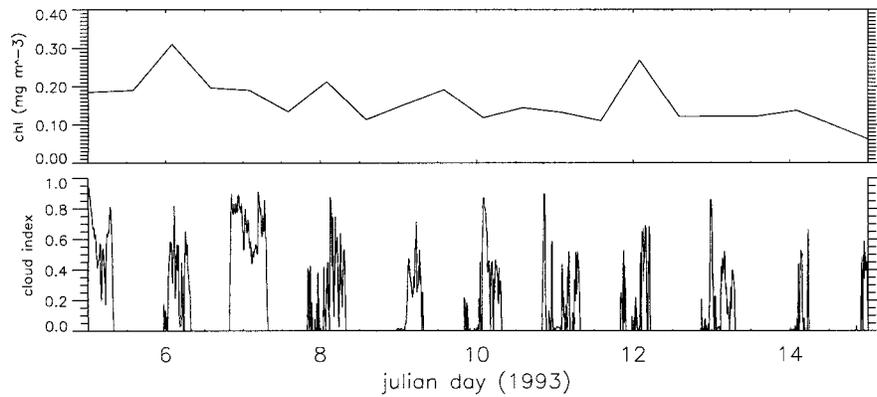

FIG. 9. Time series of upper ocean chlorophyll concentration and cloud index used to force the solar transmission parameterization presented here. Chlorophyll concentration was measured aboard the R/V *John Vickers* during TOGA COARE. Twice daily measurements are shown. Cloud index comes from normalizing incident irradiance values recorded at the IMET mooring during TOGA COARE by modeled clear-sky values.
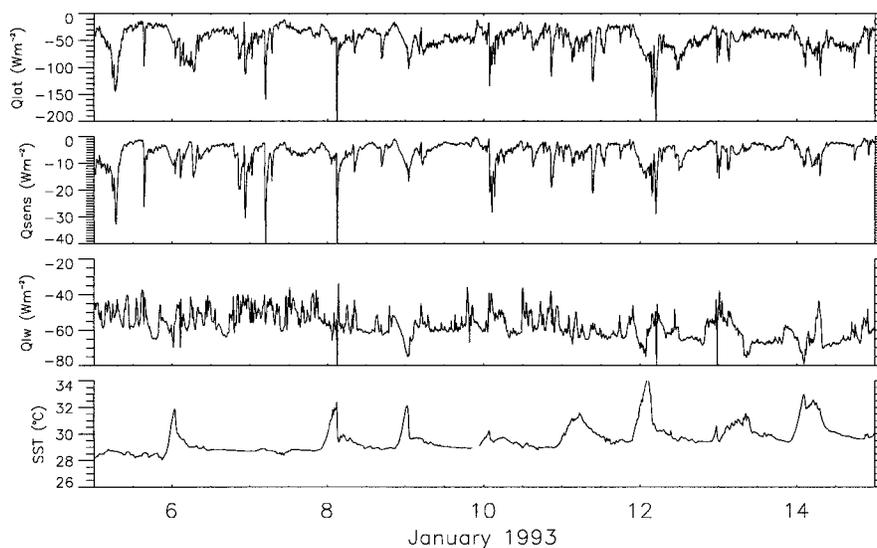
FIG. 10. Time series of latent, sensible, and longwave heat fluxes at the sea surface along with SST. Values are from the TOGA COARE bulk flux model forced with the data shown in Figs. 8 and 9, and the solar transmission parameterization described here. The time step for model runs is 7.5 min. Negative heat flux values indicate ocean heat loss.

per ocean chlorophyll concentration is available as part of the TOGA COARE bio-optical dataset recorded roughly 40 km from the IMET mooring between 21 December 1992 and 19 January 1993 aboard the R/V *John Vickers* (Siegel et al. 1995). Chlorophyll concentration was determined twice daily using standard fluorometric techniques and linearly interpolated to the 7.5-min grid of the meteorological data. For the 10-day low wind period, mean chlorophyll concentration is 0.16 mg m^{-3}, the standard deviation is 0.06 mg m^{-3}, and there is an overall decreasing trend following a large biomass increase on 4 January (Siegel et al. 1995). Cloud index is determined by normalizing incident solar radiation measurements made at the IMET mooring by clear sky irradiance values computed for the western Pacific warm pool region with the SBDART model (Ricchiazzi et al. 1998; Siegel et al. 1999; OSM). The mean value of cloud index for the period is 0.42. Mean cloud index must be interpreted cautiously because the effect of cloud index on the surface incident irradiance depends on the top-of-the-atmosphere irradiance value, which has a pronounced daily cycle. Solar zenith angle at the location of the IMET mooring is computed as a function of time and is used by the SBDART model for the calculation of incident clear sky irradiance as well as in the direct computation of transmission model parameters during clear sky periods.

Results of the TOGA COARE bulk flux model run with the two-equation solar transmission parameterization presented here are shown in Figs. 10 and 11. Time series of latent, sensible and longwave heat fluxes (Fig. 10) closely match those shown and discussed by Weller and Anderson (1996). The mean value of latent heat loss by the ocean during the low wind period (51

W m^{-2}) is less than half of the mean value for the entire IOP (Weller and Anderson 1996). Sea surface temperature (Fig. 10) increases by nearly 2°C over the 10-day study period and displays a diurnal cycle except on the cloudiest days (5, 7, and 15 January). Warm-layer depth also shows a strong diurnal cycle (Fig. 11) as nighttime convection causes deep mixing and morning sun induces stratification that slowly breaks down through the course of the day (Price at al. 1986; Fairall et al. 1996a). The fraction of the surface irradiance that is absorbed within the warm-layer ranges from 0.2 to 0.8 (Fig. 11). The warm-layer temperature correction has a mean value of 0.39°C for the 10-day study period. Cool-skin thickness is of the order of millimeters, and has a mean value of 2 mm for the study period. On average 6% of the incident surface irradiance is absorbed within the cool-skin, and the mean cool-skin temperature correction is 0.25°C (Fig. 11).

To test the sensitivity of the bulk flux model to the all-condition solar transmission parameterization presented here, the model results presented above (Figs. 10 and 11) are compared to those obtained when the COARE bulk flux algorithm is used in its original form. Differences in the resultant air–sea flux values, SST, fraction of surface irradiance heating the warm layer, warm-layer depth, warm-layer temperature correction, fraction of surface irradiance heating the cool skin, cool-skin depth, and cool-skin temperature correction are illustrated in Figs. 12 and 13. The two-equation solar transmission parameterization results in decreased latent, sensible, and longwave heat losses (Fig. 12). Mean differences in the air–sea heat fluxes for the study period are all less than 1 W m^{-2}, but instantaneous differences reach 5 and 2 W m^{-2} for the latent and longwave terms,
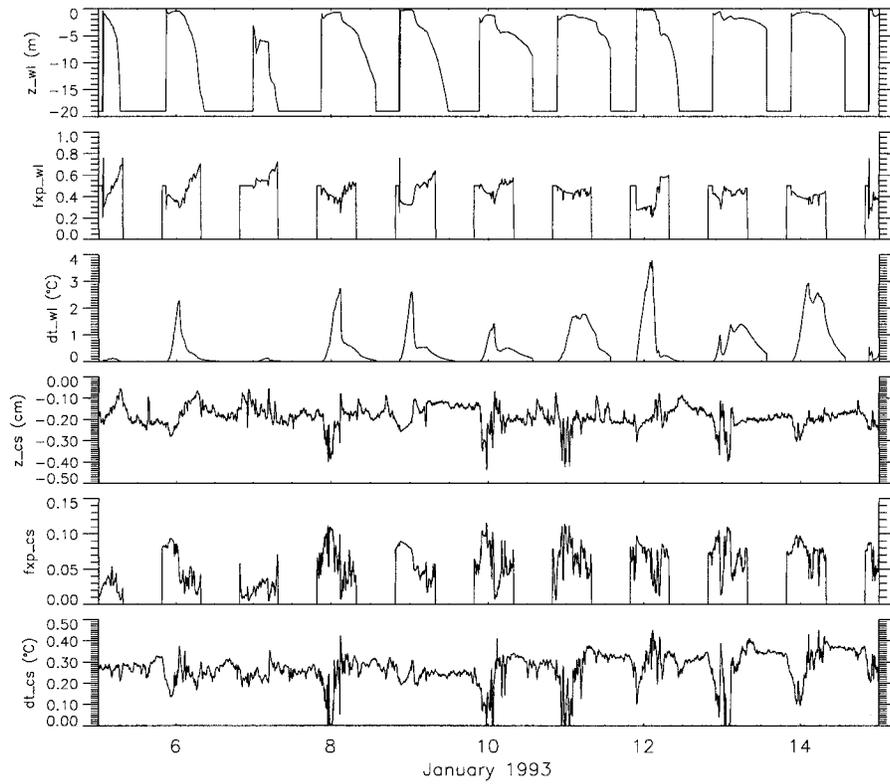
Fig. 11. Results of the TOGA COARE bulk flux model related to the transmission of solar radiation through the cool-skin and warm layer. Shown are warm-layer depth, fraction of the incident surface irradiance that is converted to thermal energy within the warm layer, and warm-layer temperature correction. Similar parameters are shown for the cool skin. Solar absorption is shown as 0 when the incident surface irradiance is less than 10 W m^{-2}. Warm-layer depth is shown as 19 m when deeper values are reached during nighttime convection (e.g., Fairall et al. 1996a).
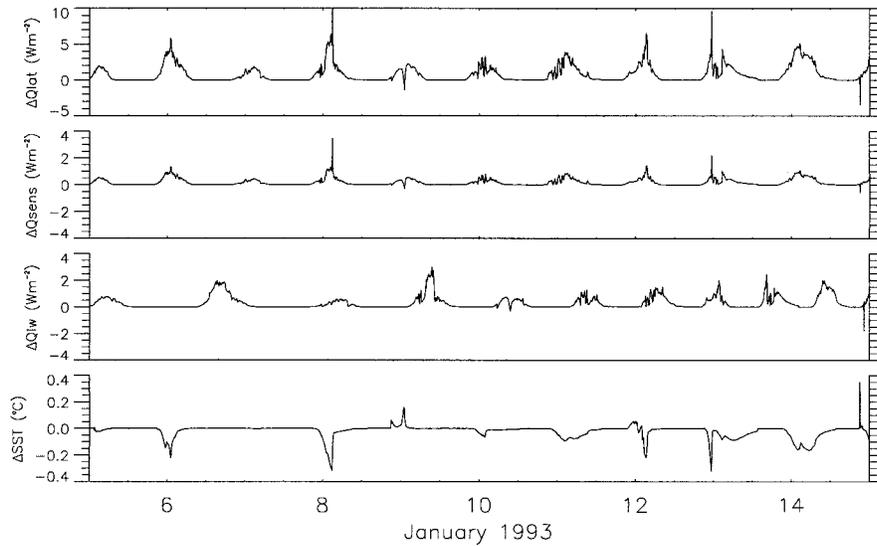

Fig. 12. Differences in air–sea heat flux values and SST (parameters shown in Fig. 10) that occur when the TOGA COARE bulk flux model is run with the physically and biologically based solar transmission parameterization developed here and compared with results using the original invariant solar transmission parameterization (new-original).
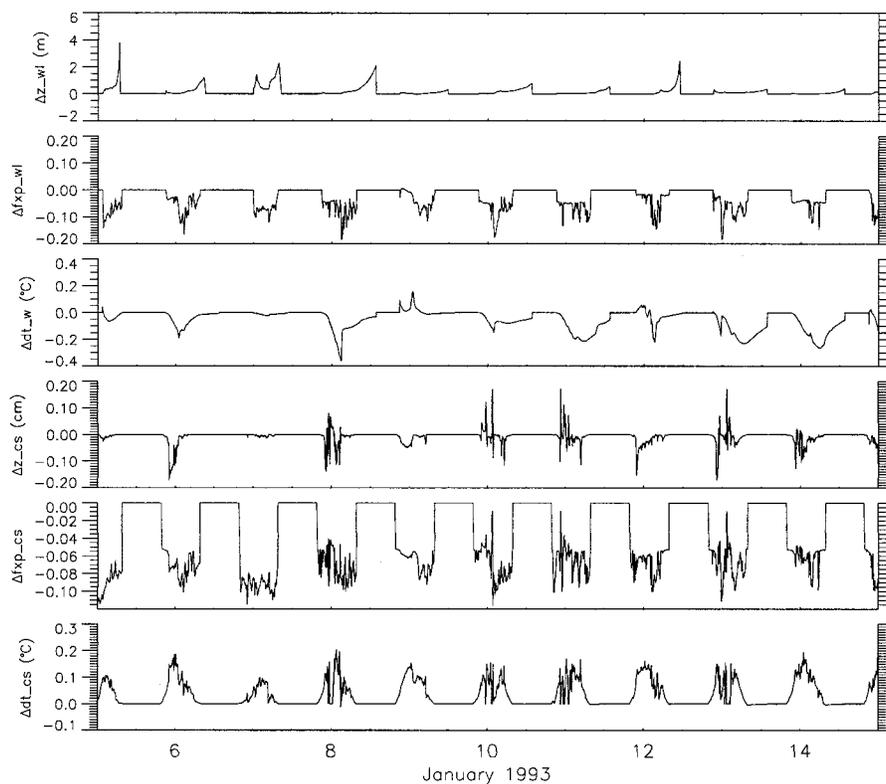
FIG. 13. Differences in the parameters shown in Fig. 11 that occur when the TOGA COARE bulk flux model is run with the physically and biologically based solar transmission parameterization developed here and compared with results using the original invariant solar transmission parameterization (new-original).

respectively. Sea surface temperature is 0.02°C cooler on average when the bulk flux model is run with the two-equation solar transmission parameterization. While nighttime convective mixing keeps the mean temperature difference small, instantaneous differences in SST reach 0.2°C for nearly half the days considered. The reduction in heat lost to the atmosphere follows the reduced SST that occurs with the improved solar transmission parameterization.

Overall, increased transmission occurs over the cool skin and warm layer with the new transmission parameterization (Fig. 13). Mean decreases in the fraction of the surface irradiance absorbed within the cool skin and warm layer are 0.07 and 0.06, respectively (mean transmission values are computed for the period when the incident surface irradiance is greater than 10 W m^{-2}), and instantaneous differences regularly exceed 0.09 and 0.15, respectively. These values suggest absolute solar flux differences that occur between the two solar transmission parameterizations are of the order 10 W m^{-2} (for daily mean values) over typical cool-skin and warm-layer depths.

A byproduct of increased solar transmission is enhanced entrainment and layer deepening as penetrating solar radiation warms underlying waters (Schneider et al. 1996; Ohlmann et al. 1998). The two-equation solar transmission parameterization gives a mean warm-layer depth increase of 0.1 m, and instantaneous differences near 2 m on nearly half the days considered (Fig. 13). Again, nighttime convection causes the warm layer to deepen keeping the mean depth difference small. The mean cool-skin depth difference for the study period is ~0. However, cool-skin depth often changes by nearly 50%, or order millimeters, when the solar transmission parameterization is altered (Fig. 13).

The differences in solar transmission and layer depth that occur with the improved solar transmission parameterization ultimately result in changed cool-skin and warm-layer temperature corrections. The average warm-layer temperature correction for the 10-day low wind period is 0.04°C less when the TOGA COARE bulk flux model is run with the two-equation solar transmission parameterization. Instantaneous temperature correction differences reach 0.2°C on half of the days considered (Fig. 13). A 0.2°C discrepancy in SST can give rise to subsequent air–sea flux errors of up to 10 W m^{-2} (Fairall et al. 1996b). The difference in warm-layer temperature correction that arises when the bulk-flux model is run with the two solar transmission parameterizations represents roughly 10% of a correction value typical of a

low wind, high insolation day (Fairall et al. 1996a). The decrease in warm-layer temperature correction for the improved solar transmission case follows the increased solar transmission and deeper warm layer. However, warm-layer temperature corrections determined with the new solar transmission parameterization are farther from the directly measured TOGA COARE values for similar conditions (Fairall et al. 1996a). This is partly due to the nonconservative handling of heat in the bulk-flux model that causes thermal energy associated with solar radiation that once penetrated the depth of the warm layer to be neglected when the warm layer deepens.

The two-equation solar transmission parameterization gives a cool-skin temperature correction greater than that for the original case, consistent with increased solar transmission in the upper ocean. The mean difference is 0.03°C, and instantaneous differences often exceed 0.1°C (Fig. 13). The cool-skin correction difference due to the change in solar transmission parameterizations represents nearly 20% of the mean cool-skin correction reported by Fairall (1996a). Cool-skin temperature corrections computed using the new solar transmission parameterization are closer to the TOGA COARE measured values (Fairall et al. 1996a). The opposite signs in cool-skin and warm-layer temperature correction differences that accompany the solar transmission parameterization change indicate an average overall decrease in the net surface temperature correction of nearly 0.1°C for high insolation, low wind periods. This result indicates that solar transmission through the near-surface layer of the ocean must be carefully considered for proper determination of the bulk temperature to SST correction, and subsequent prediction of air–sea heat fluxes.

7. Conclusions

Results from radiative transfer calculations indicate that in-water solar fluxes can vary by 40 W m^{-2} within the upper few meters of the ocean (based on a climatological surface irradiance of 200 W m^{-2}) and that a significant portion of the variation can be explained by upper ocean chlorophyll concentration, solar zenith angle, and cloud amount (OSM). Solar zenith angle is a key explanatory variable during clear sky periods, whereas cloud index, a radiometric quantification of cloud amount, is important during cloudy sky periods. Chlorophyll concentration is always important for predicting solar transmission. This study uses simulated irradiance profiles to develop an all-condition solar transmission parameterization that is physically and biologically based. The parameterization is determined empirically by fitting curves, expressed as a sum of four exponential terms, to the individual profiles. Curve-fit parameters are then written as linear combinations of chlorophyll concentration and $\cos^{-1}\theta$ during clear sky periods, and chlorophyll concentration and cloud index during cloudy sky periods. This two-equation solar transmission parameterization gives an improvement in

skill of order 10 W m^{-2} over existing full spectral parameterizations.

The solar transmission parameterization has been developed for use in all conditions typical of open ocean waters, that is, for the complete ranges of cloud cover and solar zenith angle and for upper ocean chlorophyll concentrations between 0.03 and 3.0 mg m^{-3}. The primary strength of the parameterization lies in its ability to accurately resolve solar transmission variations within the top few meters of the ocean. It is in this depth range that existing transmission parameterizations are only approximate. By implicitly including sea surface albedo, the model significantly reduces errors associated with use of a mean albedo value.

Our improved solar transmission parameterization is easily implemented in existing upper ocean models. The parameterization relies upon quantities which can be accurately determined from in situ and remotely sensed data. First, cloud index must be calculated to decide whether the clear sky or cloudy sky equation is to be used. Incident surface irradiance and clear sky irradiance (values from which cloud index is computed) can be determined from remotely sensed cloud data and simple atmospheric radiative transfer models, respectively (Tanre et al. 1979; Bishop and Rossow 1991; Ricchiazzi et al. 1998). For the cloudy sky case [Eq. (5a)], chlorophyll concentration, the remaining independent parameter, is available from remotely sensed ocean color data. For the clear sky case [Eq. (5b)], solar zenith angle and chlorophyll concentration must be determined. Solar zenith angle can be calculated from position and time-of-day information. A coded version of the all-condition solar transmission parameterization is available from the authors.

To test the influence of variations in near-surface solar transmission on upper ocean evolution and subsequent rates of air–sea heat exchange the improved transmission parameterization is incorporated into the TOGA COARE bulk flux model and results are compared with those from the original bulk flux model, which uses invariant solar transmission profiles characteristic of an arbitrary Jerlov water type. When forced with meteorological data from the western equatorial Pacific, the bulk-flux model gives roughly a 15% decrease in the quantity of solar radiation absorbed within the cool skin and warm layer when the new solar transmission parameterization is used. The 15% decrease corresponds to ~6% of the surface irradiance or an absolute flux difference of 12 W m^{-2} (for a climatological surface irradiance of 200 W m^{-2}). The increased transmission that accompanies the new transmission parameterization gives a slightly deeper warm layer and a decrease in the warm-layer temperature correction which often reaches 0.2°C. The increase in transmission over the cool skin gives an increased cool-skin temperature correction which reaches 0.1°C daily. The combined effect of the physically and biologically based solar transmission parameterization is a mean decrease in the bulk-

to-SST temperature correction of almost 0.1°C. Instantaneous changes in the temperature correction exceed 0.2°C for nearly half of the days considered. These results illustrate the need for proper resolution of solar transmission within the top few meters of the ocean to accurately predict upper ocean evolution and net air–sea heat fluxes.

REFERENCES

Bevington, P. R., and D. K. Robinson, 1992: *Data Reduction and Error Analysis for the Physical Sciences.* McGraw-Hill, 328 pp.

Bishop, J. K. B., and W. B. Rossow, 1991: Spatial and temporal variability of global surface solar irradiance. *J. Geophys. Res.,* **96,** 16 839–16 858.

Coppin, P. A., and E. F. Bradley, 1995: Ocean albedo values for TOGA-COARE: A comparison of measurements and models. *IAPSO Proceedings,* **19,** p. 428.

Cronin, M. F., and M. J. McPhaden, 1997: The upper ocean heat balance in the western equatorial Pacific warm pool during September–December 1992. *J. Geophys. Res.,* **102,** 8533–8553.

Denman, K. L., 1973: A time-dependent model of the upper-ocean. *J. Phys. Oceanogr.,* **3,** 173–184.

Efron, B., and R. J. Tibshirani, 1993: *An Introduction to the Bootstrap.* Chapman and Hall, 436 pp.

Fairall, C. W., E. F. Bradley, J. S. Godfrey, G. A. Wick, J. B. Edson, and G. S. Young, 1996a: Cool-skin and warm-layer effects on sea surface temperature. *J. Geophys. Res.,* **101,** 1295–1308.

——, ——, D. P. Rogers, J. B. Edson, and G. S. Young, 1996b: Bulk parameterization of air–sea fluxes for Tropical Ocean-Global Atmosphere–Coupled Ocean Atmosphere Response Experiment. *J. Geophys. Res.,* **101,** 3747–3764.

Gautier, C., G. R. Diak, and S. Masse, 1980: A simple physical model to estimate incident solar radiation at the surface from GOES satellite data. *J. Appl. Meteor.,* **19,** 1005–1012.

Jerlov, N. G., 1976: *Marine Optics.* Elsevier, 229 pp.

Kirk, J. T. O., 1994: *Light and Photosynthesis in Aquatic Ecosystems.* Cambridge University Press, 509 pp.

Kraus, E. B., 1972: *Atmosphere–Ocean Interaction.* Clarendon, 275 pp.

Liu, W. T., K. B. Katsaros, and J. A. Businger, 1979: Bulk parameterization of the air–sea exchange of heat and water vapor including the molecular constraints at the interface. *J. Atmos. Sci.,* **36,** 1722–1735.

Mobley, C. D., 1989: A numerical model for the computation of radiance distributions in natural waters with wind roughened surfaces. *Limnol. Oceanogr.,* **34,** 1473–1483.

——, 1994: *Light and Water.* Academic Press, 592 pp.

——, and R. W. Preisendorfer, 1988: A numerical model for the computation of radiance distributions in natural waters with wind-roughened surfaces. NOAA Tech. Memo., ERL PMEL - 75, Pacific Mar. Environ. Lab, Seattle, WA, 195 pp. [Available from NOAA/PMEL, 7600 Sand Point Way NE, Seattle, WA 98115-6349.]

Morel, A., 1988: Optical modeling of the upper ocean in relation to its biogenous matter content (case I waters). *J. Geophys. Res.,* **93,** 10 749–10 768.

——, and D. Antoine, 1994: Heating rate within the upper ocean in relation to its bio-optical state. *J. Phys. Oceanogr.,* **24,** 1652–1665.

Ohlmann, J. C., D. A. Siegel, and C. Gautier, 1996: Ocean mixed layer radiant heating and solar penetration: A global analysis. *J. Climate,* **9,** 2265–2280.

——, ——, and L. Washburn, 1998: Radiant heating of the western equatorial Pacific during TOGA-COARE. *J. Geophys. Res.,* **103,** 5379–5395.

——, ——, and C. D. Mobley, 2000: Ocean radiant heating. Part I: Optical influences. *J. Phys. Oceanogr.,* **30,** 1833–1848.

Paulson, C. A., and J. J. Simpson, 1977: Irradiance measurements in the upper ocean. *J. Phys. Oceanogr.,* **7,** 953–956.

——, and ——, 1981: The temperature difference across the cool-skin of the ocean. *J. Geophys. Res.,* **86,** 11 044–11 054.

Payne, R. E., 1972: Albedo of the sea surface. *J. Atmos. Sci.,* **29,** 959–970.

Preisendorfer, R. W., and C. D. Mobley, 1986: Albedos and glitter patterns of a wind roughened sea surface. *J. Phys. Oceanogr.,* **16,** 1293–1316.

Price, J. F., R. A. Weller, and R. Pinkel, 1986: Diurnal cycling: Observations and models of upper ocean response to diurnal heating, cooling, and wind-mixing. *J. Geophys. Res.,* **91,** 8411–8427.

Ricchiazzi, P., S. Yang, C. Gautier, and D. Sowle, 1998: SBDART: A research and teaching software tool for plane-parallel radiative transfer in the earth's atmosphere. *Bull. Amer. Meteor. Soc.,* **79,** 2101–2114.

Saunders, P. M., 1967: The temperature of the ocean–atmosphere interface. *J. Atmos. Sci.,* **24,** 269–273.

Schneider, N., T. Barnett, M. Latif, and T. Stockdale, 1996: Warm pool physics in a coupled GCM. *J. Climate,* **9,** 219–239.

Siegel, D. A., and T. D. Dickey, 1987: On the parameterization of irradiance for open ocean photoprocesses. *J. Geophys. Res.,* **92,** 14 648–14 662.

——, J. C. Ohlmann, L. Washburn, R. R. Bidigare, C. Nosse, E. Fields, and Y. Zhou, 1995: Solar radiation, phytoplankton pigments and radiant heating of the equatorial Pacific warm pool. *J. Geophys. Res.,* **100,** 4885–4891.

——, T. K. Westberry, and J. C. Ohlmann, 1999: Cloud color and ocean radiant heating. *J. Climate,* **12,** 1101–1116.

Smith, R. C., and K. S. Baker, 1978: Optical classification of natural waters. *Limnol. Oceanogr.,* **23,** 260–267.

Smyth, W. D., D. Hebert, and J. N. Moum, 1996: Local ocean response to a multiphase westerly wind burst. Part 2: Thermal and freshwater responses. *J. Geophys. Res.,* **101,** 22 513–22 533.

Soloviev, A. V., 1982: On the vertical structure of the thin surface layer of the ocean during a weak wind. *Izv. Atmos. Oceanic Phys.,* **18,** 579–585.

Tanre, D., M. Herman, P. Y. Deschamps, and A. De Leffe, 1979: Atmospheric modeling for space measurements of ground reflectances, including bidirectional properties. *Appl. Opt.,* **18,** 3587–3594.

Webster, P. J., and R. Lukas, 1992: TOGA COARE: The Coupled Ocean–Atmosphere Response Experiment. *Bull. Amer. Meteor. Soc.,* **73,** 1377–1416.

Weller, R. A., and S. P. Anderson, 1996: Surface meteorology and air–sea fluxes in the western equatorial Pacific Warm Pool during the TOGA Coupled Ocean–Atmosphere Response Experiment. *J. Climate,* **9,** 1959–1991.

Wijesekera, H. W., and M. C. Gregg, 1996: Surface layer response to weak winds, westerly bursts, and rain squalls in the western Pacific Warm Pool. *J. Geophys. Res.,* **101,** 977–997.

Woods, J. D., W. Barkmann, and A. Horch, 1984: Solar heating of the ocean—Diurnal, seasonal and meridional variation. *Quart. J. Roy. Meteor. Soc.,* **110,** 633–656.